The Crystal Structure of the Signal Recognition Particle in Complex with Its Receptor

Sandro F. Ataide,[1] Nikolaus Schmitz,[1]* Kuang Shen,[2]* Ailong Ke,[3] Shu-ou Shan,[2] Jennifer A. Doudna,[4]† Nenad Ban[1]†

Cotranslational targeting of membrane and secretory proteins is mediated by the universally conserved signal recognition particle (SRP). Together with its receptor (SR), SRP mediates the guanine triphosphate (GTP)–dependent delivery of translating ribosomes bearing signal sequences to translocons on the target membrane. Here, we present the crystal structure of the SRP:SR complex at 3.9 angstrom resolution and biochemical data revealing that the activated SRP:SR guanine triphosphatase (GTPase) complex binds the distal end of the SRP hairpin RNA where GTP hydrolysis is stimulated. Combined with previous findings, these results suggest that the SRP:SR GTPase complex initially assembles at the tetraloop end of the SRP RNA and then relocalizes to the opposite end of the RNA. This rearrangement provides a mechanism for coupling GTP hydrolysis to the handover of cargo to the translocon.

The signal recognition particle (SRP) is a ubiquitous ribonucleoprotein complex that cotranslationally delivers membrane and secretory proteins to the plasma membrane in prokaryotes and to the endoplasmic reticulum in eukaryotes (*1*, *2*). The SRP targeting process starts with recognition of a hydrophobic signal sequence on the ribosome-nascent chain complex (RNC or cargo) by the SRP to yield an RNC:SRP complex. Subsequently, the RNC:SRP complex associates on the membrane with the SRP receptor (SR). The binding between SRP and SR induces conformational changes of yet-unknown nature that allow the cargo to be transferred to the protein-conducting channel (translocon). The cycle can be resumed after guanine triphosphate (GTP) hydrolysis that drives dissociation of the SRP:SR complex (*1*–*3*).

Both the SRP and SR include components that are structurally and functionally conserved across the different domains of life (*1*, *2*). In *Escherichia coli*, SRP is composed of two universally conserved components, the Ffh protein (SRP54 in eukaryotes) and the 4.5*S* SRP RNA. Ffh contains a methionine-rich (M) domain responsible for high-affinity RNA binding and recognition of signal sequences (*4*), a helical N domain responsible for interactions with the ribosome, and a Ras-like guanine triphosphatase (GTPase) (G) domain. The *E. coli* SR is a single protein, FtsY, that consists of an N and a G domain that are structurally similar to those found in Ffh (*5*, *6*) and an additional A domain responsible for interactions with the membrane and the translocon (*7*).

When bound to GTP, SRP and SR form a stable complex through extensive interactions between their NG domains (*5*, *6*). At the heterodimer interface, a composite active site is formed in which SRP and SR act as reciprocal activating proteins for one another. GTPase activation within the SRP:SR complex is achieved by a set of conformational changes in both proteins that are distinct from those required for their initial complex assembly (*8*). Mutations that block GTPase activation severely disrupt protein targeting and translocation (*8*), suggesting that conformational changes leading to GTPase activation play an essential role in the unloading of cargo (*5*, *9*, *10*).

The RNA moiety in the SRP system is essential for cell viability in vivo (*4*, *11*) and for protein targeting and translocation in vitro (*12*, *13*). The *E. coli* 4.5*S* RNA has two characterized biochemical functions: acceleration of the interaction between Ffh and FtsY by increasing their complex assembly and disassembly rates and stimulation of GTPase activity once a stable SRP:SR complex is formed (*13*–*16*). Additionally, the SRP RNA has been described to act as a platform for conformational changes in Ffh and FtsY after recognition of the signal sequence by the M domain (*15*, *17*, *18*).

Despite extensive prior studies of cotranslational protein targeting, several fundamental questions remain unanswered: How does the SRP RNA stimulate GTP hydrolysis of the SRP:SR complex, why is this GTPase activation essential for protein targeting, and how is cargo transfer to the translocon coupled to GTP hydrolysis by Ffh and FtsY? To address these questions, we solved the three-dimensional structure of the SRP:SR complex with the nonhydrolyzable GTP analog β-γ methylene-guanosine 5′-triphosphate (GMPPCP).

The SRP:SR complex structure. The prokaryotic SRP:SR complexes were crystallized in the pre-GTP hydrolysis state (Fig. 1, A and B) (*19*, *20*). Stable complexes were assembled by using *E. coli* Ffh^{1-432}, full-length 4.5*S* RNA from *E. coli* or *Deinococcus radiodurans*, and *E. coli* $FtsY^{196-497}$ in the presence of GMPPCP and the nonionic detergent $C_{12}E_8$, which is proposed to mimic a signal peptide (*21*). Crystals of the homologous *E. coli* SRP:SR complex and the heterologous complex containing *D. radiodurans* 4.5*S* RNA were isomorphous, but the latter diffracted x-rays to higher resolution. After extensive screening, a single crystal of the heterologous complex was identified that diffracted x-rays better than others and permitted recording of a complete data set to 3.9 Å resolution (table S1). These data were used to produce an atomic-resolution model of the complex. The structure was solved by molecular replacement using high-resolution structures of isolated parts of the assembly, including the NG dimer (*5*) and the 4.5*S* RNA domain IV in complex with the M domain (*4*). Iterative rounds of rebuilding and refinement produced excellent electron density maps at 3.9 Å resolution, which allowed unambiguous tracing of the molecules and placement of side chains and bases for well-ordered parts of the structure (Fig. 1C and fig. S1). The missing parts in previous structures, specifically the distal portion of the SRP RNA and the connective linker between the NG and M domains of Ffh, could be unambiguously identified in the calculated electron density maps (omit map for the linker helix shown in Fig. 1D). The two molecules in the crystallographic asymmetric unit form a head-to-tail dimer with the N terminus of the symmetry-related Ffh molecule interacting with a groove on the M domain of the opposing molecule defined by portions of the finger loop (excluding residues 354 to 368) (*22*) (fig. S2). Electron density maps for the homologous complex calculated at 7.0 Å resolution, using the coordinates of the heterologous complex for phasing, revealed that their global structures are nearly identical (table S1, Fig. 1A, and fig. S3).

The structure shows an unexpected domain arrangement of the Ffh and FtsY proteins relative to the SRP RNA. Whereas the M domain binds near the tetraloop region (also known as helix 8 or domain IV) as observed previously (*4*), the NG heterodimer contacts the opposite end of the 4.5*S* RNA (also named helix 5) (*23*). The linker connecting the Ffh NG and M domains forms a well-defined, 30-amino-acids-long helix (Fig. 1, A and D). In previous studies, the linker region was either too flexible to be assigned (*22*) or was modeled as an α helix and a loop structure (*24*). There has been no clear evidence for a structural role of the linker helix in previous studies. However, mutations of conserved residues in the linker region abolish the ability of the SRP RNA to stimulate SRP:SR complex formation as well as GTP hydrolysis, indicating that the linker is intimately involved in the function of the SRP RNA (*17*). In the structure reported here, the linker acts as a spacer placing the activated NG domains of the Ffh and FtsY at the distal end of the 4.5*S*

[1]Institute of Molecular Biology and Biophysics, Eidgenössische Technische Hochschule Zurich (ETH Zurich), 8093 Zurich, Switzerland. [2]Division of Chemistry and Chemical Engineering, California Institute of Technology, Pasadena, CA 91125, USA. [3]Department of Molecular Biology and Genetics, Cornell University, Ithaca, NY 14853, USA. [4]Howard Hughes Medical Institute, Department of Molecular and Cell Biology, Department of Chemistry, University of California Berkeley; Physical Biosciences Division, Lawrence Berkeley National Laboratory, Berkeley, CA 94720, USA.

*These authors contributed equally to this work.
†To whom correspondence should be addressed. E-mail: ban@mol.biol.ethz.ch (N.B.); doudna@berkeley.edu (J.A.D.)

RNA. This conformation of the SRP:SR complex had not been detected previously (*15*, *25*), possibly because this configuration of the SRP:SR complex is a transient state that was stabilized by intermolecular interactions in the crystal. Nevertheless, the functional importance of this conformational state is strongly supported by the following analyses.

New function of the distal end region of the 4.5*S* RNA. In addition to the structural data presented here, another clue to the importance of the distal RNA region is its sequence conservation (Fig. 2A and fig S4). The sequence motif GUGCCG (bases 83 to 88 in *E. coli*) can be found in the helix 5 region of most known 4.5*S* RNAs (Fig. 2A) and is also conserved in the longer prokaryotic 6*S* SRP RNA (*23*). The secondary structure prediction for this region of the SRP RNA always features a bulged or unpaired base (Fig. 2A). The conservation of this region is similar to that of the SRP RNA tetraloop and the region recognized by the M domain (Fig. 2, A and B, and fig. S4).

In our structures, C83 (C86 in *E. coli*, fig. S5) is positioned close to both GMPPCP molecules and interacts directly with both Ffh and FtsY proteins at regions that regulate the GTPase activity (Fig. 2C and fig. S5) (*26*–*28*). Two residues from Ffh can form H bonds with C83, Lys^{278} interacts with the phosphate group of C83 and Glu^{277} interacts with the N4 of C83 and the 2′O from GMPPCP. In contrast, the interaction of C83 with FtsY is hydrophobic: Residues Leu^{198} and Phe^{137} stack with the base; the latter resides in the insertion box domain (IBD) motif previously described as essential for GTP binding and hydrolysis (*5*, *10*, *29*). Identical interactions have been described in the Ffh:FtsY NG domains crystal structure [Protein Data Bank (PDB) code 2CNW] containing guanine diphosphate (GDP):AlF_4, in which a peripheral nucleotide [guanine monophosphate (GMP)] was found to bind in the same position as C83 (*28*) (fig. S6). The superposition of our NG heterodimer structure with previously determined structures containing GMPPCP (PDB code 1OKK), β-γ-imido-guanosine 5′-triphosphate (GMPPNP) (PDB code 1RJ9), and GDP:AlF_4 (PDB code 2CNW) reveals no large differences in the GTPase center within the resolution limits of our structure (*5*, *6*, *26*, *27*).

The NG heterodimer exhibits an extensive interaction interface with the 4.5*S* RNA, burying 890 $Å^2$ (Fig. 3A). FtsY is responsible for the majority of these contacts, whereas Ffh interaction with the distal region of the RNA is limited to two bases, C82 and C83. However, the M domain of Ffh is also responsible for the interaction with domain IV of the 4.5*S* RNA. Taken together, the total surface area buried between Ffh and the 4.5*S* RNA is 780 $Å^2$, which is similar to the extent of interaction between FtsY and the distal portion of the 4.5*S* RNA (Fig. 3B). These observations explain why FtsY will bind the distal portion of the 4.5*S* RNA as part of the GTP-activated twin complex but not in its free state (Fig. 2C and 3B). First, the contact to the RNA is mediated by both FtsY and Ffh. Second, the local concentra-

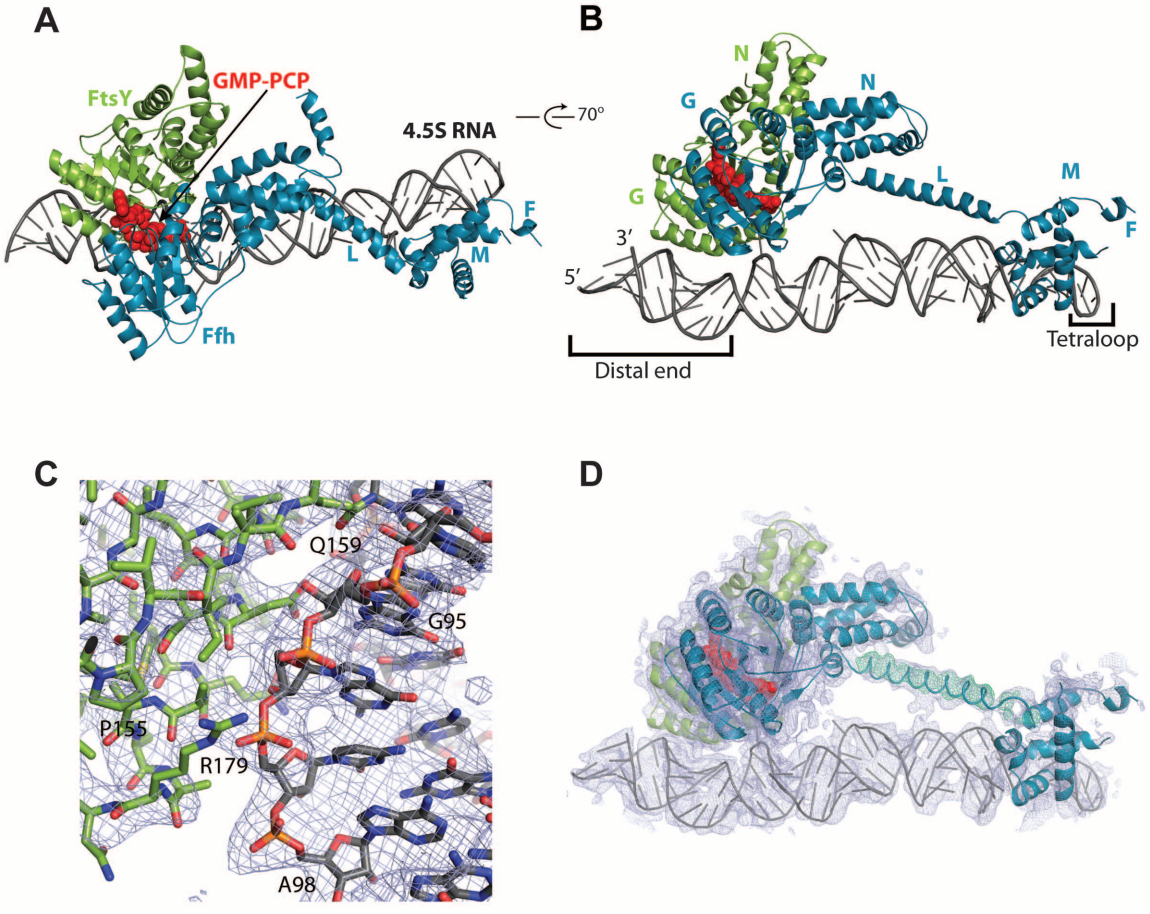

Fig. 1. Structure of SRP in complex with SR. (**A**) Top view of the SRP:SR complex. Ffh is colored blue, 4.5*S* RNA in gray, and FtsY (SR) is shown in green. The atoms of the two GMPPCP molecules are displayed as red spheres. (**B**) Side view of the SRP:SR complex rotated 70° relative to the view in (A). N denotes the N domain, G denotes the G domain, M denotes the M domain, L is the flexible linker, and F denotes the finger loop. (**C**) Visualization of the $2F_{obs} - F_{calc}$ (where F_{obs} and F_{calc} are observed and calculated structure factors, respectively) electron density contoured at 1σ and the stick representation of the SRP:SR complex (*41*). (**D**) Side view of the SRP:SR complex with the contour of a $2F_{obs} - F_{calc}$ unbiased omit map calculated for linker region residues 300 to 330 of Ffh. The linker is displayed as a tube together with the difference density $F_{obs} - F_{calc}$ electron density contoured at 3σ, shown as green mesh. The $2F_{obs} - F_{calc}$ electron density for the entire complex is contoured at 1σ and displayed as gray mesh. The cover radius used had a cutoff of 2.6 Å for the $2F_{obs} - F_{calc}$ and $F_{obs} - F_{calc}$.

tion of the tethered homodimeric NG domains is very high because they are connected via the linker region to the M domain, which is tightly bound to the SRP RNA [dissociation constant (K_D) of 5 pM] (*30*, *31*).

The SRP RNA distal end specifically stimulates GTPase activation. Although earlier work implicated the tetraloop region of the SRP RNA in GTP hydrolysis (*13*, *15*), interpretation of the observed GTPase activity is complicated by the fact that, at subsaturating protein concentrations, the observed GTPase reaction rate is limited by the assembly of the complex. Recent studies that more rigorously dissected the complex assembly versus GTP hydrolysis steps established that the tetraloop is essential for accelerating SRP:FtsY complex assembly, whereas it does not substantially affect GTPase activation once the GTPase complex is formed (*12*, *32*, *33*). To define the RNA site(s) responsible for stimulating GTP hydrolysis, we systematically truncated the *E. coli* 4.5*S* RNA from the distal end (Fig. 4A and fig. S7, A and B) and tested the effects of these mutations on the stimulated GTPase reaction between SRP and FtsY. The heterologous complex involving *D. radiodurans* 4.5*S* RNA was not used for biochemical experiments because it showed substantially lower GTPase activity. This could be either due to small differences in side chain positions at the interface of the RNA and activated NG domains, beyond the resolution limit of our current data, or due to the possibility that the experimental conditions have been optimized for measuring the activity of the *E. coli* complex. Truncations of up to 10 base pairs from the distal end did not substantially affect the GTPase rate (k_{cat}) of the SRP:FtsY complex at saturating protein concentrations (Fig. 4, B and C, and fig. S7B). However, truncation of an additional five base pairs (92mer → 82mer) reduced k_{cat} over eightfold to values approaching that observed in the absence of RNA (Fig. 4, B and C, and fig. S7B). Therefore, the base-paired region C97–C101:G10–G14 at the distal end plays an important role in the SRP RNA-mediated stimulation of GTPase hydrolysis. Consistent with these findings, this region provides a major site for docking of the SRP:SR NG domain complex at the RNA distal end (Fig. 3, A and B).

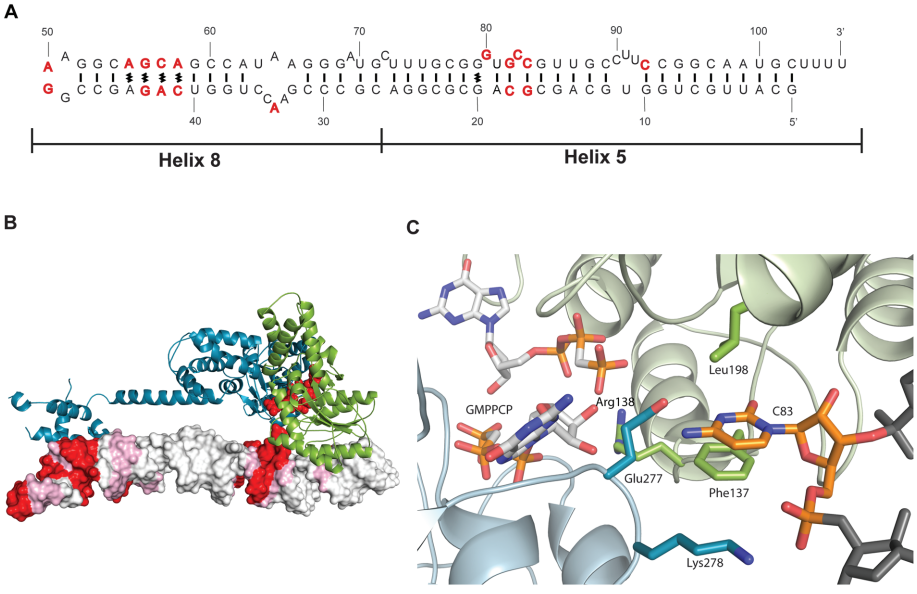

Fig. 2. Interaction of the Ffh-SR NG domain with a conserved flipped base at 5′,3′ distal end of the 4.5*S* RNA. (**A**) Secondary structure of the *D. radiodurans* 4.5*S* RNA with conserved residues indicated in red (sequence alignment displayed in fig. S4). Base pairings are indicated as straight lines and noncanonical interactions are indicated as pound symbols; bulged residues are unpaired. (**B**) Overall view of the interaction of Ffh and FtsY (displayed as ribbons and colored as in Fig. 1A) with the 4.5*S* RNA (represented as a contoured surface colored according to the conservation indicated in fig. S4). GMPPCP molecules are shown as red spheres. (**C**) Closeup view of the interaction of the conserved flipped C83 with the interface of Ffh and FtsY. 4.5*S* RNA is displayed as sticks colored in gray with C83 colored in orange. Ffh and FtsY residues that interact directly with C83 are displayed as sticks and colored as in (B). GMPPCP residues are represented as sticks colored with white carbons, red oxygens, blue nitrogens, and orange phosphates.

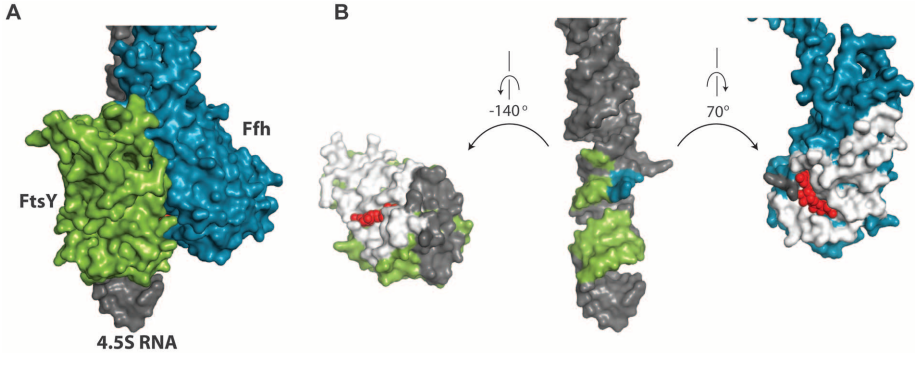

Fig. 3. Major contact area of the Ffh:FtsY NG domain with 5′,3′ region of the 4.5*S* RNA. (**A**) Surface representation of the SRP:SR complex in the 5′,3′ region of the 4.5*S* RNA. (**B**) Surface representation of the separated Ffh and FtsY (rotate each to one direction) from the 4.5*S* RNA [maintained in the same orientation as in (A)]. The interface between Ffh and FtsY is displayed in white in both proteins with GMPPCP displayed as red spheres. The contact area of each protein to the RNA is indicated in gray. The FtsY contact area in the RNA is indicated in green and the Ffh contact area in blue; C83 is indicated in blue but contacted by both proteins.

In contrast, the values of k_{cat}/K_m (where K_m is the Michaelis constant) in the stimulated GTPase reaction were largely unaffected unless the SRP RNA was truncated to less than 56 nucleotides (Fig. 4B and fig. S7B). Because the k_{cat}/K_m value in this reaction rate is limited by SRP:FtsY complex formation (*19*), this result strongly argues that the distal end accelerates the actual GTP catalysis step but not the initial SRP:FtsY complex assembly. To provide independent evidence for this possibility, we directly measured the complex assembly rate constants by using acrylodan conjugated at Ffh-C235, a probe that changes fluorescence upon formation of a GTP-dependent SRP:FtsY complex (*19*). SRP:FtsY complex assembly rates were affected no more than twofold for RNA truncations up to the 56mer; a substantial defect was detected only with the 43mer (Fig. 4D and fig. S7C). Therefore, the distal end of the SRP RNA specifically stimulates GTPase activation in the SRP:FtsY complex without affecting the initial assembly of the complex. Together with previous work (*12*, *32*, *33*), these results demonstrate that the SRP RNA contains two separate motifs that regulate distinct stages of the SRP:FtsY interaction: The tetraloop end accelerates the initial assembly of the complex, whereas the distal end facilitates GTPase activation at late stages.

To test the role of the extruded base C86 in GTPase activation, we either removed C86 (ΔC86) or mutated it to A, G, or U. Deletion of C86 or its mutation to G reduced the GTPase rate constant by half, whereas the C86A and C86U mutations reduced GTPase activity by factors of 7 to 10, to rates approaching that in the absence of the SRP RNA (Fig. 4E and fig. S7D). These data

support a role of the extruded base in modulating GTPase activity and explain the conservation of the identity of this base.

Modeling the conformation of the SRP:SR on the ribosome. The data presented here, together with previous structural and biochemical studies, show that the SRP complex can exist in distinct conformational states depending on the orientation of the linker between the NG and M domains of Ffh. We propose that these conformational states represent different stages of the SRP-mediated protein targeting pathway. Indeed, the large rearrangement of the NG domains from their initial position in the vicinity of the 4.5*S* RNA tetraloop as observed in electron microscopy (EM) and biochemical studies (*15*, *18*, *34*, *35*) to the opposite end of this RNA suggests a plausible mechanism of transferring the RNC from the SRP to the translocon. In order to better understand the implications of the observed conformational changes in the targeting process, we modeled our structure onto the ribosome by using available cryogenic EM (cryo-EM) data (*34*) (Fig. 5A). The SRP bound to the RNC in the absence of the SR is in a conformation in which its NG domain is next to the M domain with the linker region wrapping around the M domain (Fig. 5B) (*24*, *34*, *36*). We propose that the structure described here represents the cargo-release state of the protein targeting cycle. Repositioning the NG domains of Ffh and FtsY to the distal region of 4.5*S* RNA exposes ribosomal proteins L23 and L29, which constitutes the main translocon binding site. Therefore, this conformational change simultaneously exposes the signal sequence-binding cleft of the M domain and liberates the translocon binding region on the ribosome (*36*–*38*).

Because the SRP cycle is evolutionarily conserved, we speculate that many of the molecular features that govern the prokaryotic SRP cycle will also occur in eukaryotes. Upon comparison of the molecular model in Fig. 5 with the cryo-EM density of the eukaryotic RNC:SRP:SR complex arrested with the GTP analog GMPPNP, certain similarities can be observed (*37*). Most noticeable, in the eukaryotic complex the density for the NG domains of the SRP54 and SR proteins (homologous to Ffh) is absent from the tetraloop end of the 4.5*S* RNA, whereas additional density appears in the distal end of the SRP RNA as observed in our complex (fig. S8). It is therefore possible that this density originates from the activated twin NG domains rather than from SR alone, as suggested (*37*).

The SRP cycle revised. On the basis of these data, a mechanism can be envisioned that governs the handoff of substrates to the translocon and the role of GTP in this process. The initial interaction of free SRP with the RNC involves binding of the N domain of Ffh to the ribosomal proteins L23 and L29 (Fig. 6A) as well as interaction of the M domain of Ffh with the signal sequence, possibly aided by the linker helix that wraps around the M domain in the RNC-bound

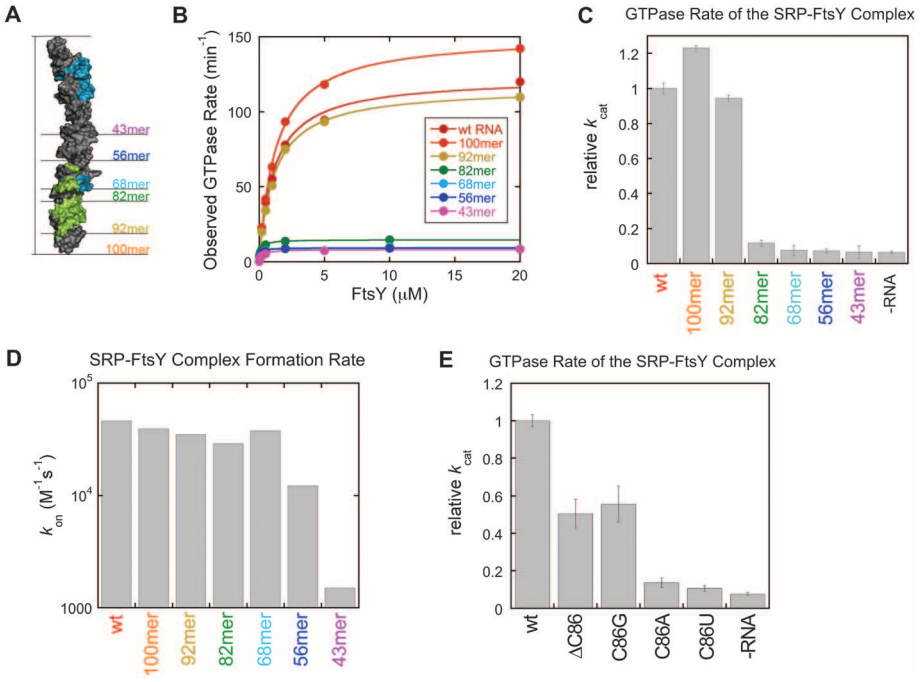

Fig. 4. The SRP RNA distal end specifically stimulates GTP hydrolysis in the SRP:SR complex. (**A**) *E. coli* SRP RNA systematically truncated from the distal end that were used in this study (see fig. S7A for the sequence of the truncated RNA constructs). The FtsY contact area in the RNA is indicated in green and the Ffh contact area in blue; C86 is indicated in blue but contacted by both proteins. (**B**) Stimulated GTPase activity between SRP and FtsY with the SRP RNA mutants in (A). The data were fit to the Michaelis-Menten equation, and the kinetic constants k_{cat} and k_{cat}/K_m are summarized in fig. S7B. wt, wild type. (**C**) A substantial defect in the GTPase rate of the SRP:FtsY complex was observed upon truncation of the SRP RNA from the 92mer to 82mer. Rate constants were from (B) and normalized to that of the wild-type SRP RNA. Error bars indicate SDs from two independent experiments. (**D**) Truncation of the RNA distal end did not substantially affect SRP-FtsY complex formation rates (k_{on}) until the C loop is truncated (43mer). Values of k_{on} were derived from fig. S7B. (**E**) Mutation of the conserved base C86 (C83 in *D. radiodurans* 4.5*S* RNA) impairs the ability of SRP RNA to stimulate GTPase hydrolysis of the SRP:FtsY complex. Rate constants were relative to that of the wild-type SRP RNA and were derived from the data in fig. S7D. Error bars indicate SDs from three independent experiments.

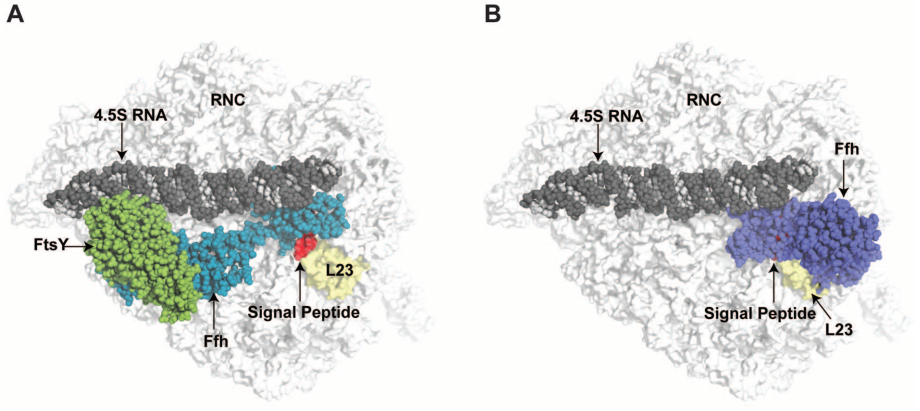

Fig. 5. Conformation of the SRP and SRP:SR structure on the ribosome showing the large rearrangement between cargo-binding and cargo-release modes. (**A**) The structure of the SRP:SR is superimposed on the SRP:RNC bound structure from cryo-EM reconstruction (*34*), with Ffh in the cryo-EM structure omitted. The signal peptide from the SRP:RNC structure was maintained (red surface) as a reference for the exit tunnel. The RNC is displayed as a white surface with the protein L23 highlighted in yellow. SRP:SR are presented as spheres, with 4.5*S* RNA colored with dark gray for phosphate and ribose and light gray for bases; Ffh is blue and FtsY is green. (**B**) The cargo-binding conformation of SRP in the SRP:RNC model structure from cryo-EM is indicated as spheres with Ffh colored in purple.

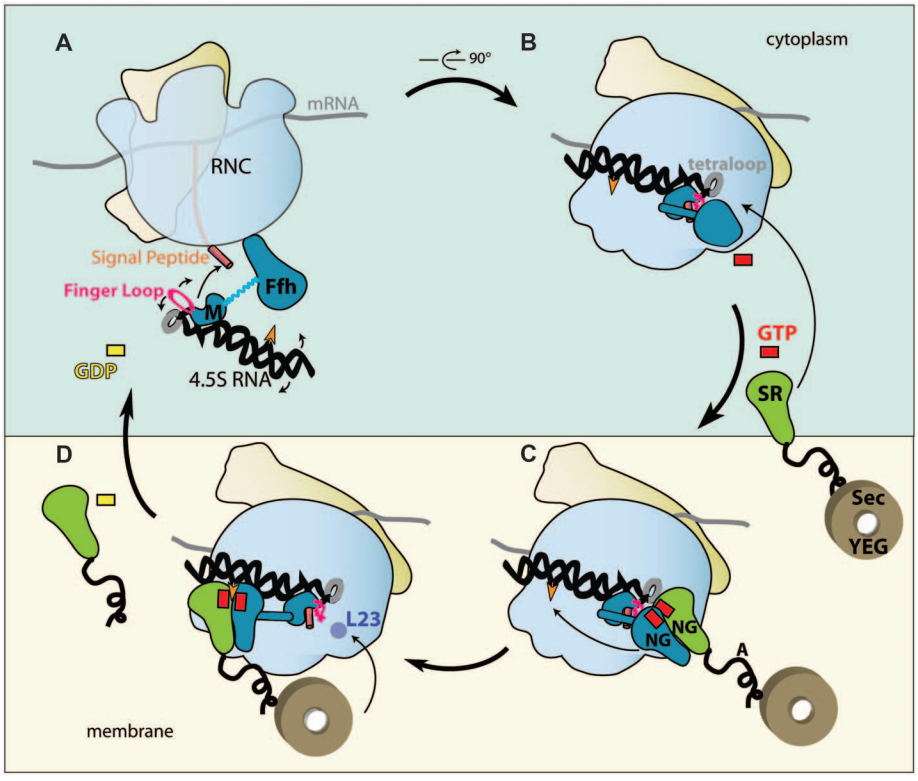

Fig. 6. Model of the SRP targeting cycle. Schematic depiction of the sequence of conformational changes involved in the SRP cycle (viewed in the membrane plane). (**A**) SRP recognizes the RNC and M domain interacts with the signal peptide (finger loop is indicated in pink). (**B**) The N domain interacts with L23, and the linker region folds on top of the signal peptide covering/shielding the M domain. (**C**) SRP bound cargo (RNC) is transferred to the membrane vicinity via SRP interaction with SR. (**D**) GTP-dependent rearrangements in the SRP:SR complex enables detachment of the Ffh N domain from L23 and the RNA tetraloop, and the NG domain complex relocates to the 5′,3′ end of the 4.5*S* RNA sandwiching the C83 (orange arrowhead) at the interface of the two G domains. This repositioning simultaneously exposes the signal sequence bound to the M domain and the L23 region of the ribosome for interactions with the translocon (Sec YEG), which is associated with the A domain of FtsY (black tail). In the final step, signal sequence is transferred from the M domain to the translocon, and the distal region of the 4.5*S* RNA promotes GTP hydrolysis and subsequent Ffh and FtsY dissociation.

conformation of the SRP (Fig. 6B) (*34*, *36*). In this RNC preorganized state, the Ffh G domain is positioned in the vicinity of the tetraloop end of the 4.5*S* RNA and primed for interaction with the SR (Fig. 6B) (*15*, *16*, *34*–*36*). Receptor binding is initially facilitated by the RNA tetraloop (*13*, *14*, *32*, *39*), which stabilizes an early conformation of the heterodimeric NG complex through interaction with the SR (Fig. 6C) (*5*, *10*, *16*). Subsequent structural rearrangements in the GTPase complex may reduce the affinity of the RNA tetraloop for the SR as well as that of the Ffh N domain for the ribosome (Fig. 6C) (*5*, *6*, *37*). Consequently, the activated NG heterodimer detaches from the ribosome exit site, but stays tethered to the SRP RNA via the tightly bound M domain and relocates to the alternative binding site at the distal end of the 4.5*S* RNA hairpin (Fig. 6D). Because the A domain of FtsY associates with the translocon (*7*, *40*), repositioning of the NG domain heterodimer will carry the translocon toward its ribosome binding site (L23), which is now exposed (Fig. 6D). This repositioning could also stabilize the linker domain in the extended helical conformation away from the M domain, thus exposing the signal sequence-binding cleft for peptide release to the translocon. Concurrently, the interaction of the activated NG heterodimer with the distal portion of the 4.5*S* RNA will stimulate GTPase activity in both Ffh and FtsY, leading to their dissociation and completing the targeting cycle (Fig. 6D).

The conformation of the SRP in complex with its receptor observed here also explains many previous observations, including the density features observed in the cryo-EM reconstruction of the eukaryotic RNC:SRP:SR complex (*37*) and the observation that mutations that disrupt the conformational changes leading to GTPase activation block late stages of protein targeting (*8*). Previous studies also indicated that overexpression of a truncated 4.5*S* RNA (domain IV) is capable of sustaining cell viability in a 4.5*S* depleted strain (*4*). According to the model described here, signal sequence transfer would be possible even in the absence of the distal region of the SRP RNA because the reduced GTPase rate would provide a longer time frame for the less-efficient signal sequence transfer to occur.

The results presented here, together with previous biochemical evidence (*13*–*18*, *21*), define the SRP RNA as a bifunctional molecule acting as a binding platform for the initial receptor interactions on one end of the 142 Å long molecule and for the activated GTPase domains of the Ffh:FtsY complex on the other end. Such conformational change provides a mechanism for the temporal and spatial exchange of large factors that have to access the signal sequence as it emerges from the ribosomal exit tunnel.

References and Notes

1. R. J. Keenan, D. M. Freymann, R. M. Stroud, P. Walter, *Annu. Rev. Biochem.* **70**, 755 (2001).
2. J. A. Doudna, R. T. Batey, *Annu. Rev. Biochem.* **73**, 539 (2004).
3. U. Kutay, G. Ahnert-Hilger, E. Hartmann, B. Wiedenmann, T. A. Rapoport, *EMBO J.* **14**, 217 (1995).
4. R. T. Batey, R. P. Rambo, L. Lucast, B. Rha, J. A. Doudna, *Science* **287**, 1232 (2000).
5. P. F. Egea *et al.*, *Nature* **427**, 215 (2004).
6. P. J. Focia, I. V. Shepotinovskaya, J. A. Seidler, D. M. Freymann, *Science* **303**, 373 (2004).
7. S. Angelini, S. Deitermann, H. G. Koch, *EMBO Rep.* **6**, 476 (2005).
8. S. O. Shan, S. Chandrasekar, P. Walter, *J. Cell Biol.* **178**, 611 (2007).
9. S. O. Shan, P. Walter, *Proc. Natl. Acad. Sci. U.S.A.* **100**, 4480 (2003).
10. S. O. Shan, R. M. Stroud, P. Walter, *PLoS Biol.* **2**, e320 (2004).
11. H. Wood, J. Luirink, D. Tollervey, *Nucleic Acids Res.* **20**, 5919 (1992).
12. X. Zhang, S. Kung, S. O. Shan, *J. Mol. Biol.* **381**, 581 (2008).
13. F. Y. Siu, R. J. Spanggord, J. A. Doudna, *RNA* **13**, 240 (2007).
14. P. Peluso, S. O. Shan, S. Nock, D. Herschlag, P. Walter, *Biochemistry* **40**, 15224 (2001).
15. R. J. Spanggord, F. Siu, A. Ke, J. A. Doudna, *Nat. Struct. Mol. Biol.* **12**, 1116 (2005).
16. L. F. Estrozi, D. Boehringer, S. O. Shan, N. Ban, C. Schaffitzel, *Nat. Struct. Mol. Biol.* **18**, 88 (2011).
17. N. Bradshaw, P. Walter, *Mol. Biol. Cell* **18**, 2728 (2007).
18. S. B. Neher, N. Bradshaw, S. N. Floor, J. D. Gross, P. Walter, *Nat. Struct. Mol. Biol.* **15**, 916 (2008).
19. X. Zhang, C. Schaffitzel, N. Ban, S. O. Shan, *Proc. Natl. Acad. Sci. U.S.A.* **106**, 1754 (2009).
20. Materials and methods are available as supporting material on *Science* Online.
21. N. Bradshaw, S. B. Neher, D. S. Booth, P. Walter, *Science* **323**, 127 (2009).
22. C. Y. Janda *et al.*, *Nature* **465**, 507 (2010).
23. C. Zwieb, N. Larsen, *Nucleic Acids Res.* **20** (suppl.), 2207 (1992).
24. K. R. Rosendal, K. Wild, G. Montoya, I. Sinning, *Proc. Natl. Acad. Sci. U.S.A.* **100**, 14701 (2003).
25. I. Buskiewicz *et al.*, *J. Mol. Biol.* **351**, 417 (2005).
26. C. L. Reyes, E. Rutenber, P. Walter, R. M. Stroud, *PLoS ONE* **2**, e607 (2007).
27. J. Gawronski-Salerno, D. M. Freymann, *J. Struct. Biol.* **158**, 122 (2007).
28. P. J. Focia, J. Gawronski-Salerno, J. S. Coon 5th, D. M. Freymann, *J. Mol. Biol.* **360**, 631 (2006).
29. S. O. Shan, P. Walter, *Biochemistry* **44**, 6214 (2005).
30. U. Schmitz *et al.*, *RNA* **2**, 1213 (1996).
31. R. T. Batey, J. A. Doudna, *Biochemistry* **41**, 11703 (2002).
32. J. R. Jagath *et al.*, *RNA* **7**, 293 (2001).
33. K. Shen, S. O. Shan, *Proc. Natl. Acad. Sci. U.S.A.* **107**, 7698 (2010).
34. M. Halic *et al.*, *Nature* **444**, 507 (2006).
35. M. Halic *et al.*, *Nature* **427**, 808 (2004).
36. C. Schaffitzel *et al.*, *Nature* **444**, 503 (2006).

37. M. Halic *et al.*, *Science* **312**, 745 (2006).
38. K. Mitra *et al.*, *Nature* **438**, 318 (2005).
39. J. R. Jagath, M. V. Rodnina, W. Wintermeyer, *J. Mol. Biol.* **295**, 745 (2000).
40. B. Weiche *et al.*, *J. Mol. Biol.* **377**, 761 (2008).
41. Single-letter abbreviations for the amino acid residues are as follows: A, Ala; G, Gly; Q, Gln; and R, Arg.
42. We thank K. Zhou for excellent technical assistance and help with crystal preparation during the early stages of the project. Initial crystallographic analysis was performed at beamline 8.2.2 at the Advanced Light Source (ALS), Lawrence Berkeley National Laboratory; we acknowledge C. Ralston for outstanding technical assistance at the ALS. Crystallographic data were collected at the beamline X06SA at the Swiss Light Source (SLS). We thank A. Brunger for the prerelease version of CNS and for helpful comments on the refinement, C. Schulze-Briese and T. Tomizaki for their outstanding support at the SLS, T. Maier and S. Klinge for critical discussion and reading of the manuscript, and T. Maier and M. Leibundgut for help and assistance with data collection and solving the structure. S.F.A. was funded initially by the Howard Hughes Medical Institute and currently by an ETH postdoctoral fellowship, N.S. is funded by Boehringer Ingelheim Fonds, and K.S. is funded by NIH grant GM078024 to S.S. This work was supported in part by the Howard Hughes Medical Institute (J.A.D.) and by the Swiss National Science Foundation (SNSF) and the National Center of Excellence in Research (NCCR) Structural Biology program of the SNSF. Atomic coordinates and structure factors for the SRP:SR crystal structure have been deposited with the Protein Data Bank under accession code 2xxa.

Supporting Online Material
www.sciencemag.org/cgi/content/full/331/6019/881/DC1
Materials and Methods
Figs. S1 to S8
Tables S1 and S2
References

13 August 2010; accepted 18 January 2011
10.1126/science.1196473

REPORTS

Metallic and Insulating Oxide Interfaces Controlled by Electronic Correlations

H. W. Jang,[1] D. A. Felker,[2] C. W. Bark,[1] Y. Wang,[3] M. K. Niranjan,[3] C. T. Nelson,[4] Y. Zhang,[4,5] D. Su,[6] C. M. Folkman,[1] S. H. Baek,[1] S. Lee,[1] K. Janicka,[3] Y. Zhu,[6] X. Q. Pan,[4] D. D. Fong,[7] E. Y. Tsymbal,[3] M. S. Rzchowski,[2] C. B. Eom[1]*

The formation of two-dimensional electron gases (2DEGs) at complex oxide interfaces is directly influenced by the oxide electronic properties. We investigated how local electron correlations control the 2DEG by inserting a single atomic layer of a rare-earth oxide (*RO*) [(*R* is lanthanum (La), praseodymium (Pr), neodymium (Nd), samarium (Sm), or yttrium (Y)] into an epitaxial strontium titanate oxide ($SrTiO_3$) matrix using pulsed-laser deposition with atomic layer control. We find that structures with La, Pr, and Nd ions result in conducting 2DEGs at the inserted layer, whereas the structures with Sm or Y ions are insulating. Our local spectroscopic and theoretical results indicate that the interfacial conductivity is dependent on electronic correlations that decay spatially into the $SrTiO_3$ matrix. Such correlation effects can lead to new functionalities in designed heterostructures.

Advanced deposition techniques enable the growth of epitaxial heterostructures with atomically controlled interfaces such as multilayers (*1*), superlattices (*2*–*4*), and ultrathin films (*5*, *6*). In these artificial structures, the interfaces play a prominent role in determining the functionalities of the structures and their applications (*7*). A recent example is the discovery of two-dimensional electron gases (2DEGs) at the interface between complex insulating oxides (*8*) such as $LaAlO_3/SrTiO_3$ (*9*, *10*), $LaTiO_3/SrTiO_3$ (*2*), and $LaVO_3/SrTiO_3$ (*11*) heterostructures, in which the 2DEG is confined near the LaO/TiO_2 interface. Magnetic and superconducting ground states of the 2DEG have been identified (*12*–*14*), and applications to field-effect transistors and tunnel junctions have been demonstrated (*15*–*17*).

Theoretical work on $LaTiO_3/SrTiO_3$ superlattices (*18*) suggests that for a several-unit-cell-thick $LaTiO_3$ layer, the $LaTiO_3/SrTiO_3$ interface region is metallic; however, nonmetallic behavior dominates in the $LaTiO_3$ region away from the interface, resulting from strong electron correlations similar to those found in bulk $LaTiO_3$. In other bulk rare-earth titanates, the effect of electron correlations depends critically on the rare-earth ion (*19*). We used the unique electronic character of oxide interfaces, and atomic level control of their structure and composition, to deliberately manipulate the 2DEG electronic properties.

We studied the effect of strong electron correlations on an oxide 2DEG by inserting a single atomic layer of *RO* (*R* is La, Pr, Nd, Sm, or Y) into an epitaxial $SrTiO_3$ matrix using pulsed-laser deposition with atomic layer control. The *RO* layer donates electrons to the conduction band of $SrTiO_3$. These electrons remain near the inserted *RO* layer due to Coulomb attraction. We find that the transport properties of these electrons range from metallic to insulating, depending critically

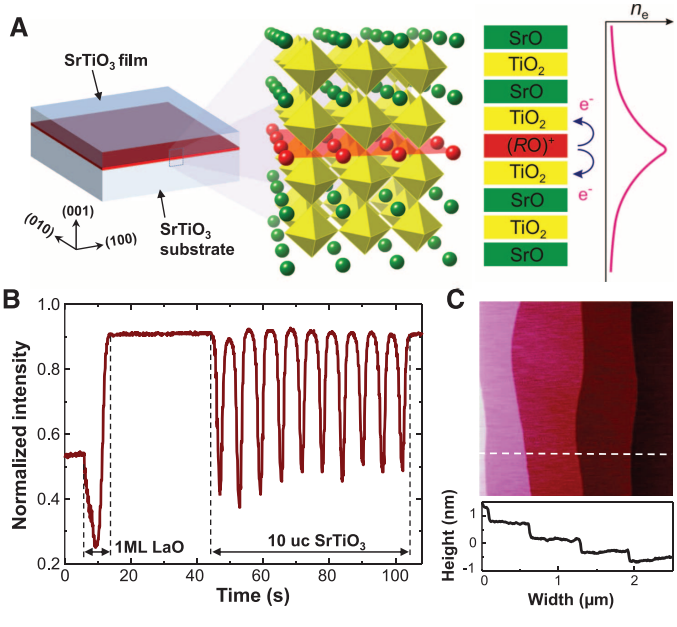

Fig. 1. (**A**) Schematic representation of a $SrTiO_3$/1-ML *RO*/$SrTiO_3$ heterostructure. The atomic structure near the interface is enlarged. The +1 valent *RO* layer donates electrons to neighboring TiO_2 planes, leading to the larger electron density n_e near the interface. (**B**) Typical RHEED oscillations for the growth of 1-ML LaO and 10-uc $SrTiO_3$ layers in sequence on a TiO_2-terminated $SrTiO_3$ substrate. (**C**) AFM image of a 10-uc $SrTiO_3$/1-ML $LaO/SrTiO_3$ heterostructure showing an atomically smooth surface.

[1]Department of Materials Science and Engineering, University of Wisconsin–Madison, Madison, WI 53706, USA. [2]Department of Physics, University of Wisconsin–Madison, Madison, WI 53706, USA. [3]Department of Physics and Astronomy, Nebraska Center for Materials and Nanoscience, University of Nebraska–Lincoln, Lincoln, NE 68588, USA. [4]Department of Materials Science and Engineering, University of Michigan–Ann Arbor, Ann Arbor, MI 48109, USA. [5]National Laboratory of Solid State Microstructures and Department of Materials Science and Engineering, Nanjing University, Nanjing 210093, P.R. China. [6]Center for Functional Nanomaterials, Brookhaven National Laboratory, Upton, NY 11973, USA. [7]Materials Science Division, Argonne National Laboratory, Argonne, IL 60439, USA.

*To whom correspondence should be addressed. E-mail: eom@engr.wisc.edu.